Continuous Detuning of an Optical Cavity with a Universally Tunable Modulator

by

Emily Davis

Submitted to the Department of Physics
in partial fulfillment of the requirements for the degree of

Bachelor of Science in Physics

at the

MASSACHUSETTS INSTITUTE OF TECHNOLOGY

June 2012

Author .....
Department of Physics
May 18, 2012

Certified by .....
Nergis Mavalvala
Department of Physics
Thesis Supervisor

Accepted by .....
Professor Nergis Mavalvala
Senior Thesis Coordinator, Department of Physics

Continuous Detuning of an Optical Cavity with a Universally Tunable Modulator

by

Emily Davis

Submitted to the Department of Physics
on May 18, 2012, in partial fulfillment of the
requirements for the degree of
Bachelor of Science in Physics

Abstract

It is currently well-known how to lock an optical cavity on resonance using the Pound-Drever-Hall technique. It is also possible to lock a cavity at a single detuned length using an amplitude modulated laser beam. However, there are many interesting applications, that would benefit from the use of a Universally Tunable Modulator (UTM), because it can create any ratio of amplitude to phase modulation. The unique transfer function of the UTM allows for cavity locking at any of the intermediate points between resonance and about half a linewidth of detuning. In this thesis, we construct such a UTM and verify experimentally that the modulator can indeed be used for continuous detuning of optical cavities.

Thesis Supervisor: Nergis Mavalvala
Title: Department of Physics

Acknowledgments

I would like to thank Professor Mavalvala for giving me the opportunity to work on such a great project at MIT-LIGO. It was a wonderful experience to work with both her and her group, to see how the lab operates, and most importantly to learn so much cool physics! I would also like to thank her for taking the time to make all her helpful comments on this thesis and motivating me to write it in the first place. Outside of lab, she was also a wonderful mentor and gave plenty of useful advice. I was very lucky to have had the chance to work with her.

This thesis would not have been written without the help of all the research scientists and grad students at MIT-LIGO. I would like to thank Sam Waldman, who showed me how to align the cavity, made me use the scope probes, and helped me find the materials for and build the tank circuits. Shannon Sankar helped me to find components, align optics, and understand mode matching code and mode spacing, among many other things. Tomoki Isogai suffered through mode matching with me, helping me to make the beam scan measurements, choose lenses, and align the beam. Tim Bodiya answered lots and lots of questions and helped me get started on the phase shifting circuit boards, as well helping me to look at Labjack data and to use his mode matching code. Eric Oelker helped me find lots of optics, helped me to use his version of mode matching code, and allowed me to borrow various books on lasers and optics. Thank to Chris Wipf, Peter Fritschel, and Richard Mittleman for answered various questions, helping me to find components, and showing me how to operate the laser. Thanks so much to all of you for helping me to learn and for having the patience to instruct an inexperienced undergraduate!

Contents

List of Figures

Chapter 1

Introduction

While phase and amplitude modulators are commonly used for a wide range of optical applications, there is no commercially available device that can perform both phase and amplitude modulation in any desired ratio of modulation depths. However, for reasons that will be explained, such a device would be useful in experiments that incorporate detuned optical cavities, such as the ponderomotive interferometer experiment currently being carried out by the quantum measurement group at MIT-LIGO [5, 4]. This device is called a Universally Tunable Modulator (UTM) and was first prototyped by Cusack, et al [7]. It can be continuously tuned from pure amplitude to pure phase modulation by shifting the relative phase of two independent voltage inputs. Another UTM was constructed at MIT-LIGO by Sarah Ackley for her senior thesis [1]. I have worked on preparing the UTM for insertion into the ponderomotive interferometer experiment.

1.1 Optical Cavities

A linear optical cavity is a resonator consisting of a pair of reflecting mirrors. Incident laser light, which can be approximated as a plane wave, bounces back and forth between the reflectors and can be resonantly enhanced when the round trip phase is an integer multiple of 2π. Because a laser beam is not perfectly point-like but in fact has finite transverse width, the cavity resonant modes also have a field pattern across

the surface of the reflector. The transverse eigenmodes of the cavity remain constant in relative shape and relative phase after having traversed a round trip through the cavity. Such modes are commonly referred to as the TEM_{00}, TEM_{10}, TEM_{11}, and so forth, as shown in Figure 1-1. Each transverse mode has an associated set of longitudinal modes satisfying the condition $\lambda = 2ln$, where l is the cavity length, λ is the wavelength of the light in the cavity medium (in this experiment, air), and n is an integer. Waves that are not eigenmodes of the cavity have a very high loss, so they radiate away quickly and contribute negligibly to the power circulating in the cavity.

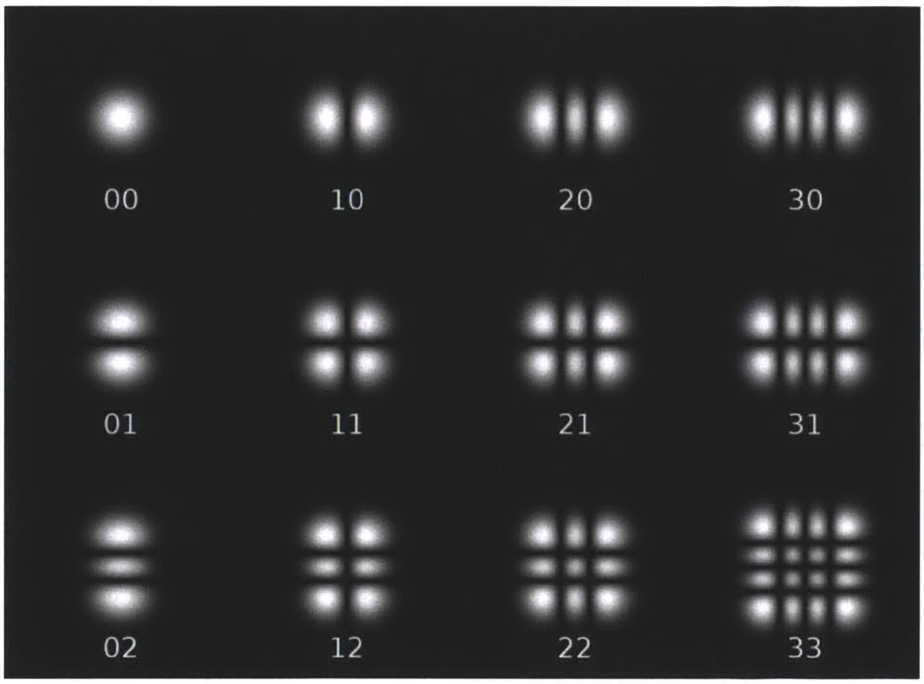

Figure 1-1: Various TEM modes. This image was created by graduate student Keenan Pepper and is freely available under the Creative Commons License.

The properties of a cavity with flat mirrors are determined by the reflectivities and spacing of the mirrors. The reflection coefficient of a cavity of length l is given by

$$F(\omega) = \frac{-r_1 + r_2 e^{-i(\omega/c)2d}}{1 - r_1 r_2 e^{-i(\omega/c)2d}} \tag{1.1}$$

where r_1 and r_2 are the amplitude reflection coefficients of the input and output mirrors, respectively, and ω is the frequency of the incoming light. The expression $\omega d/c$

can equivalently, and perhaps more revealingly, be written as $2\pi d/\lambda$, but Equation 1.1 is better kept in terms of ω for calculating the reflected error signal in Section 2.3.4.

Cavities are sometimes categorized as under-coupled, critically coupled, and over-coupled based on the relationship between r_1 and r_2. Over-coupled cavities have a greater amplitude reflection coefficient at the output mirror, $r_2 > r_2$. On resonance, essentially all of the incident light is reflected. Critically coupled cavities have equal amplitude reflection coefficients, $r_1 = r_2$, and reflect no light on resonance.

The transmission through a simple Fabry-Perot cavity can easily be extracted from the reflection coefficient:

$$T = 1 - |F(\omega)|^2 = \frac{(1-R_1)(1-R_2)}{[1-(R_1R_2)^{1/2}]^2 + 4(R_1R_2)^{1/2}\sin^2(\omega d/c)} \tag{1.2}$$

where $R_1 = r_1^2$ and $R_2 = r_2^2$ are the reflectivities of the two mirrors, and d is the length of the cavity. The transmission is plotted for several values of R_1 and R_2 in Figure 1-2.

Two common parameters used to characterize cavities are the *free spectral range*, or FSR, and the *finesse*, $\mathcal{F}$. The FSR is the frequency spacing between adjacent transmission peaks of a single transverse mode, and is given by

$$\Delta f = \frac{c}{2\sqrt{\epsilon_r \mu_r} d} \tag{1.3}$$

The finesse $\mathcal{F}$ is the ratio of the FSR to the full-width half-maximum of the transmission peaks $\Delta f_{1/2}$:

$$\mathrm{F} = \frac{\text{free spectral range}}{\text{full width at half-maximum}} = \frac{c/2d}{\Delta f_{1/2}} = \frac{\pi(R_1R_2)^{1/4}}{1-(R_1R_2)^{1/2}} \tag{1.4}$$

Qualitatively, the higher the finesse, the narrower the transmission peaks. Some of the properties of the flat-mirror cavity change when one or both of the cavity mirrors become spherical. To efficiently couple the laser light into the cavity, it is necessary to make the transverse mode of the incident laser beam match the cavity eigenmode, as is discussed in Section 2.3.3. Flat-mirror cavities are unstable, and are rarely used

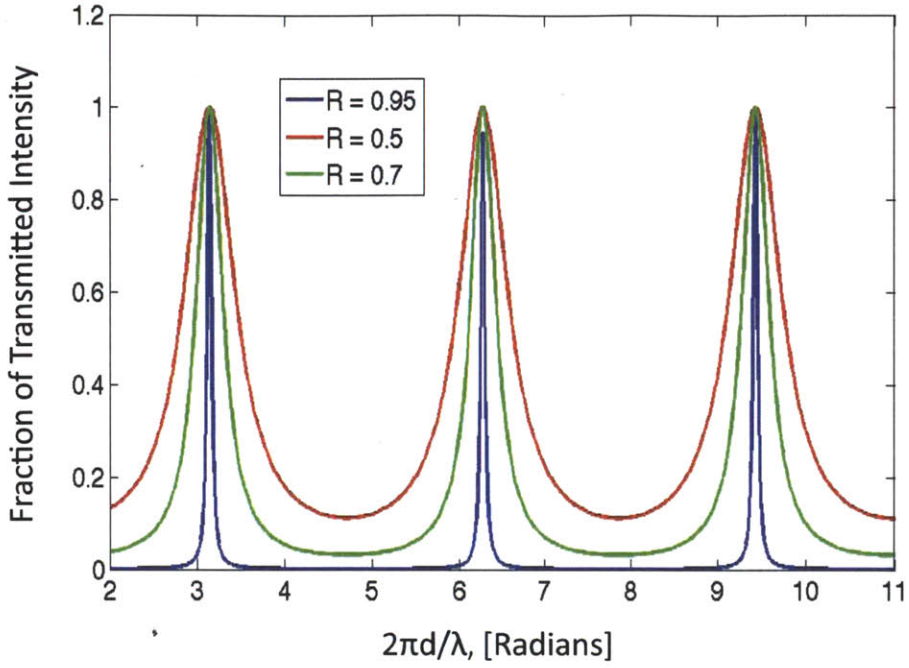

Figure 1-2: The transmission through a Fabry-Perot cavity, plotted for values of $R_1 = R_2 = 0.5$, 0.7, and 0.95.

in practice. More often mirrors with spherical curvature are used to construct high finesse optical cavities.

1.2 Pound-Drever-Hall Locking

The Pound-Drever-Hall (PDH) method is a technique that was invented to aid in frequency stabilization of lasers [2, 8]. However, it can also be used to lock an optical cavity at a certain desired cavity length d_0 such that the input light of frequency ω_0 is at resonance in the cavity. Locking is accomplished through the use of a negative feedback loop, such as the one depicted in Figure 1-3, which automatically adjusts for small disturbances to the system. An input laser beam is phase-modulated at some frequency ω_m and sent into the cavity, although some of it is reflected by the input mirror; the exact amount depends on $\delta d = d - d_0$, as well as the properties of the

cavity. The reflected light is detected on a photodiode, mixed with a local oscillator at ω_m, and low-pass filtered, which allows the desired error signal to be extracted, as shown in Figure 1-4. Some amplification of the signal or other adjustments might be needed in order to obtain the correct actuation, so the signal is passed through a servo amplifier. The feedback signal is finally applied to a piezoelectric crystal on one of the cavity mirrors, which changes the cavity length towards d_0. Clearly, the

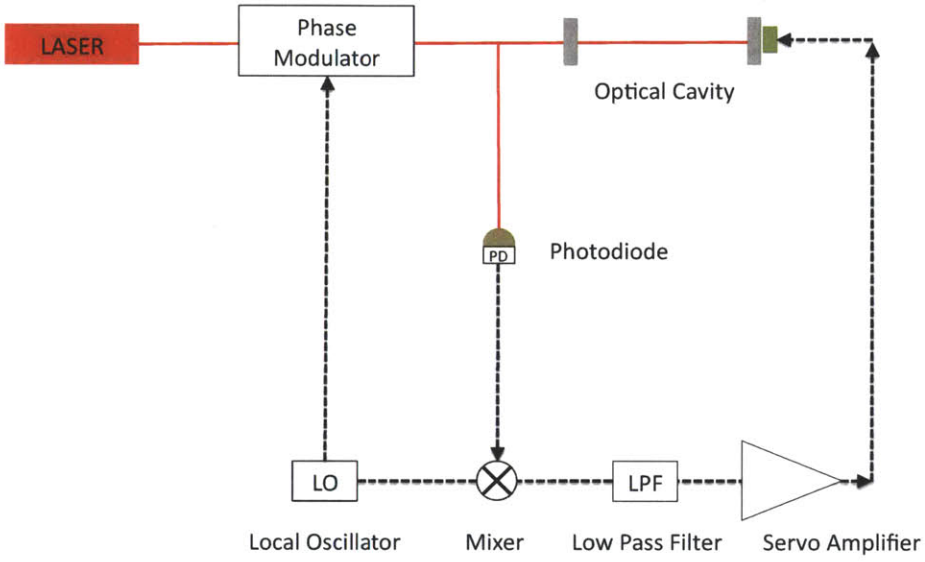

Figure 1-3: The signal chain for a Pound-Drever-Hall negative feedback loop.

reflected signal in Figure 1-4 changes sign as it passes through resonance, meaning that a feedback loop that drives the error signal to zero will push the cavity length towards d_0. However, there are some cases where we would prefer to lock the cavity off-resonance. The use of a UTM, as we shall show, allows us to make a slight variation on the PDH locking method that shifts the zero-crossing in the feedback signal so we can lock at a point slightly off-resonance such that the optical cavity is detuned.

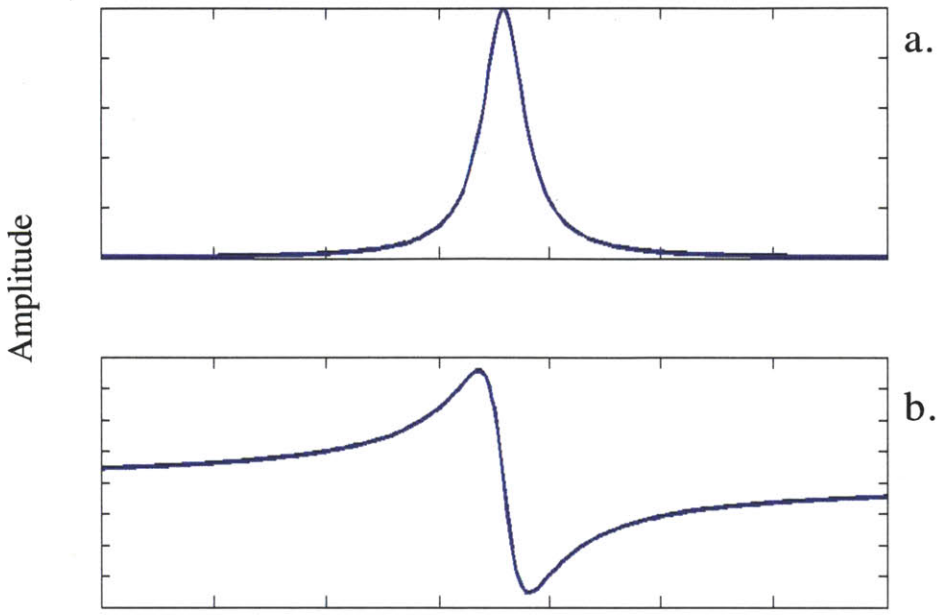

Figure 1-4: a. The transmission through a cavity swept through resonance. b. The corresponding reflected error signal used in the Pound-Drever-Hall method.

1.3 Application to the Ponderomotive Interferometer

The quantum measurement group of MIT-LIGO works on experiments that that explore interesting properties of optomechanical systems [5, 4]. One of the objectives of the experiment is to cool 1 gram mirrors down to temperatures on the order of 10 nK, with the goal of seeing quantum effects in macroscopic objects [6].

Mirror cooling can be achieved with an optical trap that utilizes optical springs [3]. When a cavity is locked on resonance, there is no force caused by radiation pressure (to first order). However, if the cavity is slightly detuned from the resonance, the radiation pressure becomes linear with respect to small changes in cavity length. If the cavity is lengthened, the radiation pressure will push the mirror farther away; if the cavity is shortened, the radiation pressure will restore the mirror to its

original position. This optical restoring force changes the resonant frequency of the mirror oscillator, an effect that has been measured: the resonant frequency of a 250 gram mirror was shifted from 1 Hz to 80 Hz, and a 1 gram mirror oscillator's resonant frequency was shifted from 172 Hz to 5 kHz [3].

Because the cavity has some length, the fields inside actually respond to length changes with some time delay that gives rise to a velocity-dependent damping force. This leads to a damping force that counteracts the optical spring. Combining two such optical springs at different detuning levels creates a stable optical trap for the mirrors [3].

Chapter 2

A Universally Tunable Modulator

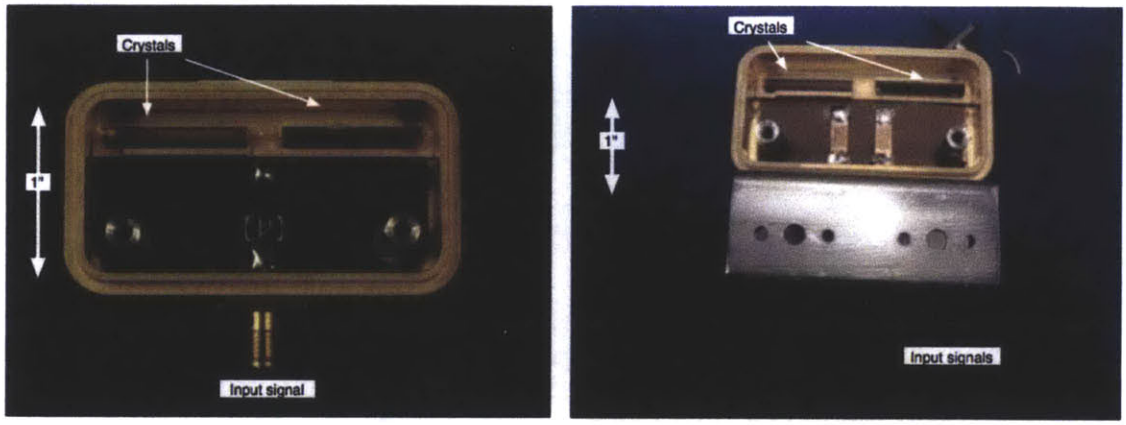

Figure 2-1: The UTM. It is shown from the top before and after the modifications made by Sarah for her thesis [1]. The modulating crystals are clearly visible.

The UTM was constructed by modifying a commercially available New Focus amplitude modulator (model 4140). The original modulator consisted of two lithium niobate crystals with their polarization angles rotated 90° with respect to each other, driven by a single input signal. Sarah disconnected the electrical connection between the two crystals and created a custom-made circuit board such that each crystal has its own input, so they can be independently controlled [1]. The orientation of the two crystals is depicted in Figure 2-2. The laser beam propagates down the z-axis, but the voltage is applied in a direction perpendicular to the$z$-axis. Two identical crystals are used to eliminate the effects of thermal drift; even if the length of the crystals

changes with temperature, each polarization component passes through equal path lengths along both axes.

Cusack, et al derive the transfer function for the UTM in Appendix A of [7], which is given by

$$\tilde{P} = \frac{E_{in}}{2}\cos(\frac{\sigma}{2})(\tilde{\delta_1} + \tilde{\delta_2}), \tag{2.1}$$

$$\tilde{A} = \frac{E_{in}}{2}\sin(\frac{\sigma}{2})(\tilde{\delta_1} - \tilde{\delta_2}), \tag{2.2}$$

Where $\tilde{P}$ and $\tilde{A}$ are the strength of the phase and amplitude modulation, respectively; σ is the angle between the two polarization components exiting the UTM, and $\tilde{\delta_1}$ and $\tilde{\delta_2}$ are the input signals. The amount of modulation can be changed by increasing or decreasing the magnitude of the input signals, while the proportion of amplitude to phase modulation can be changed by adjusting the phase between the input signals.

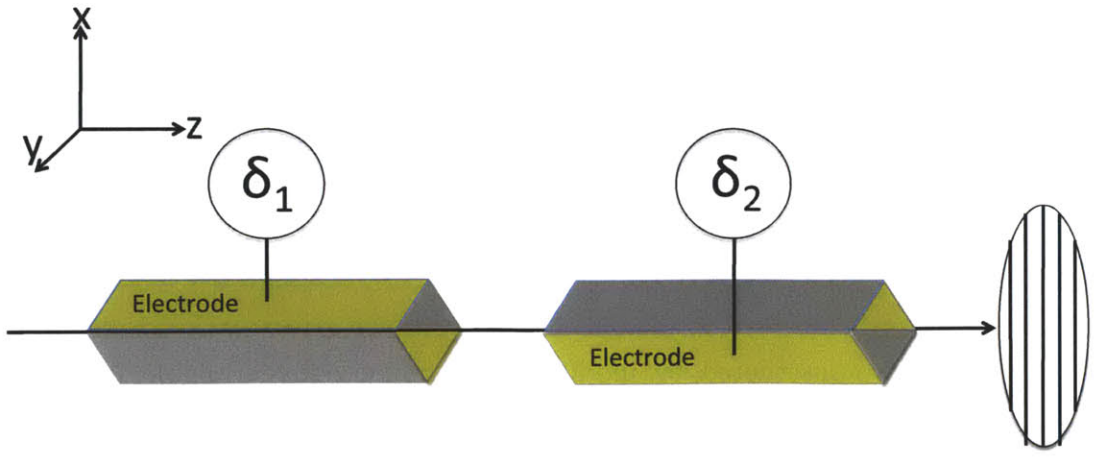

Figure 2-2: The two lithium niobate crystals lie inside the modulator box with their polarization axes and electrode contacts rotated 90° with respect to each other. Each crystal has its own separate input signal, δ_1 or δ_2, which in this setup are two phase-shifted 25 MHz sinusoidal waves. The direction of light propagation through the crystals is shown with the black arrow. The modulator is followed by a linear polarizer which is an essential part of the amplitude modulation.

2.1 The Linear Electrooptic Effect

The lithium niobate crystals are anisotropic, meaning that they have a dielectric tensor $\epsilon(\vec{r})$ which is not constant throughout the crystal, and instead changes depending on the axis [10]. For a crystal with no external voltage applied, we can choose basis vectors $\vec{x}, \vec{y}$, and $\vec{z}$ such that $\epsilon(\vec{r})$ is diagonal, and we call these vectors the principle coordinate axes. In this basis, we have

$$\begin{pmatrix} D_x \\ D_y \\ D_z \end{pmatrix} = \begin{pmatrix} \epsilon_x & 0 & 0 \\ 0 & \epsilon_y & 0 \\ 0 & 0 & \epsilon_z \end{pmatrix} \begin{pmatrix} E_x \\ E_y \\ E_z \end{pmatrix}$$

Then the stored electric energy density can be easily written as

$$8\pi E_e = \vec{E} \cdot \vec{D} = \frac{D_x^2}{\epsilon_x} + \frac{D_y^2}{\epsilon_y} + \frac{D_z^2}{\epsilon_z} \tag{2.3}$$

Substituting $x_k = D_k/\sqrt{8\pi E_e}$ and $n_k^2 = \epsilon_k$, where n_k is the index of refraction along the k axis, we then obtain the equation for the index ellipsoid:

$$1 = \frac{x^2}{n_x^2} + \frac{y^2}{n_y^2} + \frac{z^2}{n_z^2} \tag{2.4}$$

When an external electric field is applied to the crystals, it changes the principle axes such that, in general, $\epsilon(\vec{r})$ is no longer diagonal in the original basis. The change in $\epsilon(\vec{r})$, to linear order, is called the linear electrooptic effect. We can calculate what an applied voltage does to our crystals using the measured electrooptic coefficients r_{ij} for $LiNbO_3$ from the literature, and work on the linear electrooptic effect by Pockels. In our modulator, $n_x = n_y = n_0$. When an arbitrary electric field is applied to the crystal, the index ellipsoid becomes

$$\begin{aligned} 1 = (\frac{1}{n_0^2} + r_{13}E_z - r_{22}E_y)x^2 + (\frac{1}{n_0^2} + r_{22}E_y + r_{13}E_z)y^2 + (\frac{1}{n_z^2} + r_{33}E_z)z^2 \\ +2r_{42}E_y yz + 2r_{42}E_x xz - 2r_{22}E_x xy \end{aligned} \tag{2.5}$$

If only E_x is applied to the crystal, as it is in this setup, we obtain new sets of principle axes and refraction indices by finding the eigenvectors and eigenvalues of the above matrix equation with $E_z = E_y = 0$. We can then calculate the induced phase difference between different components of the incident light.

2.2 Amplitude and Phase Modulation

Amplitude modulation refers to a change in the amplitude of a signal. Given some sinusoidal carrier wave $c(t) = A\sin(\omega_c t + \phi)$, we can modulate it by multiplying by a modulation signal $m(t) = M\sin(\omega_m t + \phi)$, yielding $y(t) = AM\sin(\omega_m t + \phi)\sin(\omega_c t + \phi)$. Plotting such a signal yields Figure 3-2a. The amount of amplitude modulation can be characterized by the modulation depth, which is defined as M/A. In an experiment, amplitude modulation of laser light can be observed by shining the light on a fast photodetector.

Phase modulation refers to a time-varying change in the phase of a signal. Given some sinusoidal carrier wave $c(t) = A\sin(\omega_c t + \phi)$, phase modulation is described by adding some function in the argument, yielding the modulated signal $y(t) = A\sin(\omega_c t + m(t) + \phi)$. Plotting such a signal yields Figure 3-2b. This signal is plotted in the time domain. in frequency space, the signal at $c(t)$ gains two sidebands at frequency components $w_c \pm w_m$, with a height determined by the modulation depth, as depicted in Figure 2-4. In an experiment, phase modulation of laser light can be observed by looking at the sidebands on the transmission through an optical cavity.

2.2.1 Universal Modulation

Universal modulation is some combination of amplitude and phase modulation in any ratio. If the carrier signal is again given as $c(t) = \sin(\omega_c t)$, we can obtain a modulated signal $y(t) = A(t)\sin(\omega_c t + m(t))$. Arbitrary ratios are achieved in this experiment through the use of the UTM's unique transfer function for the light passing through it. A signal that can be both phase and amplitude modulated creates a useful reflected signal from an optical cavity as we shall explore in a later section.

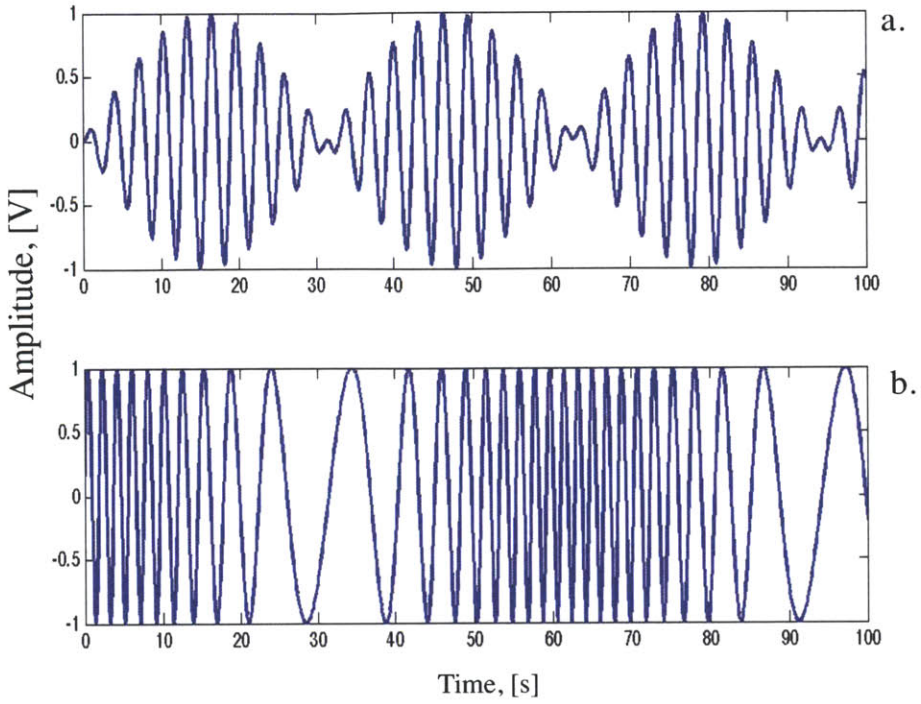

Figure 2-3: a) A carrier signal with amplitude modulation. b) A carrier signal with phase modulation.

2.3 Experimental Setup

The experimental setup is shown in Figure 2-6. A 1064 nm Nd:YAG laser first illuminates a half-wave plate and then passes through a polarizing beam-splitter (PBS). This setup allows the amount of light propagating through the experiment to be controlled when the half-wave plate is turned. Most of the power is dumped, but about 10 mW of linearly polarized light is allowed to propagate further. The light passes through a quarter-wave plate, which adjusts the input polarization to the UTM. Normally we would like the light to become circularly polarized in order to distribute power equally into the amplitude and phase modulation, as can be easily seen by the transfer functions in Equation 2.2. The light then passes through a lens which focuses it to a smaller waist, allowing the beam to pass through the UTM's small aperture. A second lens placed at the output keeps the spot size constant as the light propagates further.

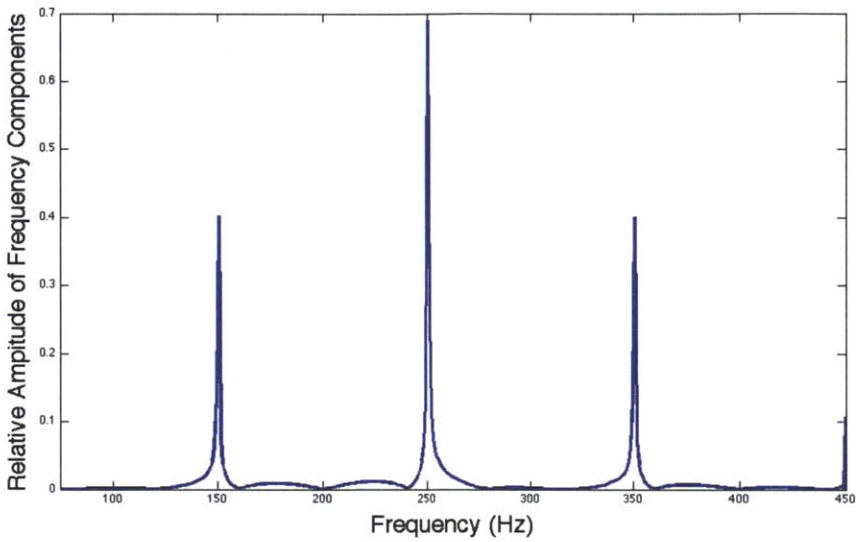

Figure 2-4: A phase modulated signal has been Fourier transformed into the frequency domain. The large central peak is the carrier frequency. The two sidebands are located at $f_c \pm f_m$ with a height determined by the modulation depth.

The electrical input to the UTM comes from a crystal oscillator at 25.23 MHz, which is split, then amplified by two voltage-controlled ZFL-1000G amplifiers. One of the inputs is given some phase shift relative to the other by adding a length of cable. For example, a 180° shift can be obtained by adding $\lambda/2$, or about 4 meters, of cable. The inputs are then passed through two resonant circuits attached to the two inputs of the UTM.

After being modulated in the UTM, the light is again split by a PBS. Path A, as indicated in Figure 2-6 is used to measure the amplitude modulation. A fast photodiode (1811) is placed in the beam path, and the variations in light intensity are captured. Path B goes to the cavity. It passes through a quarter-wave plate and becomes circularly polarized. The light then passes through two mode-matching lenses and enters the cavity, whose length is swept using a voltage-controlled piezo-electric crystal. A photodiode is placed at the output in order to view the transmission. Path

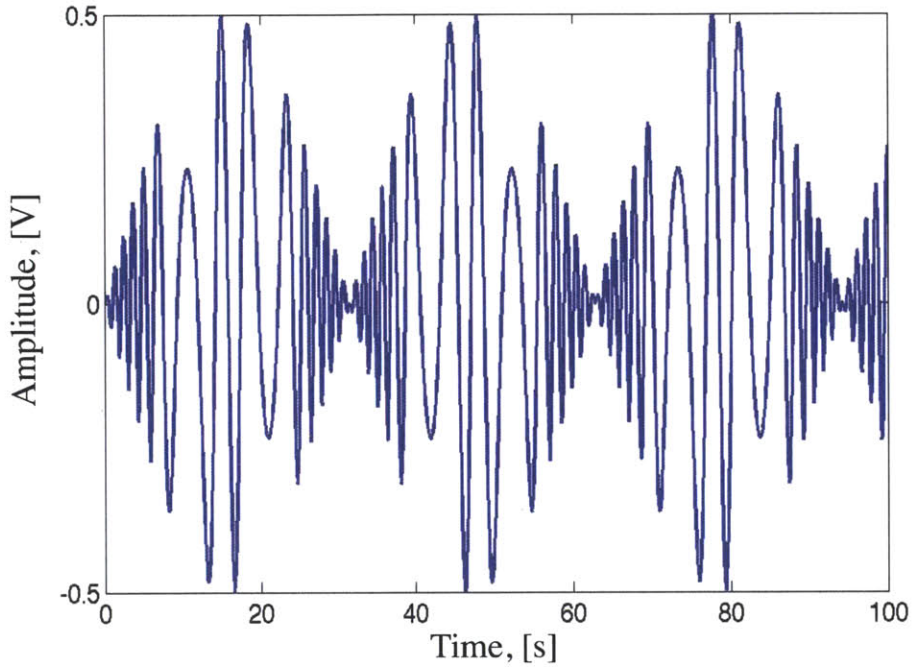

Figure 2-5: A carrier signal with both phase and amplitude modulation.

C is used to look at the reflected signal from the cavity. The reflected signal travels back along Path B, and becomes linearly polarized when it passes back through the quarter-wave plate so that it can pass completely through the PBS and reach the fast photodiode, another 1811. (Another advantage of this setup is that it prevents any light from getting reflected back towards the laser.)

The AC-coupled signal is mixed with the local oscillator signal at 25.23 MHz and low-passed so that the DC component of this signal can be viewed on an oscilloscope.

2.3.1 Resonant Circuit Construction and Measurements

After the experiment was constructed, it was still impossible to see any sidebands on the light transmitted through the optical cavity. The V_π on the modulator's crystals is 300 V, but the maximum input electrical power is 10 W. Because the allowable input power was relatively small, we couldn't just amplify the input voltages in order to obtain the necessary voltages across the crystal to get an appreciate amount of

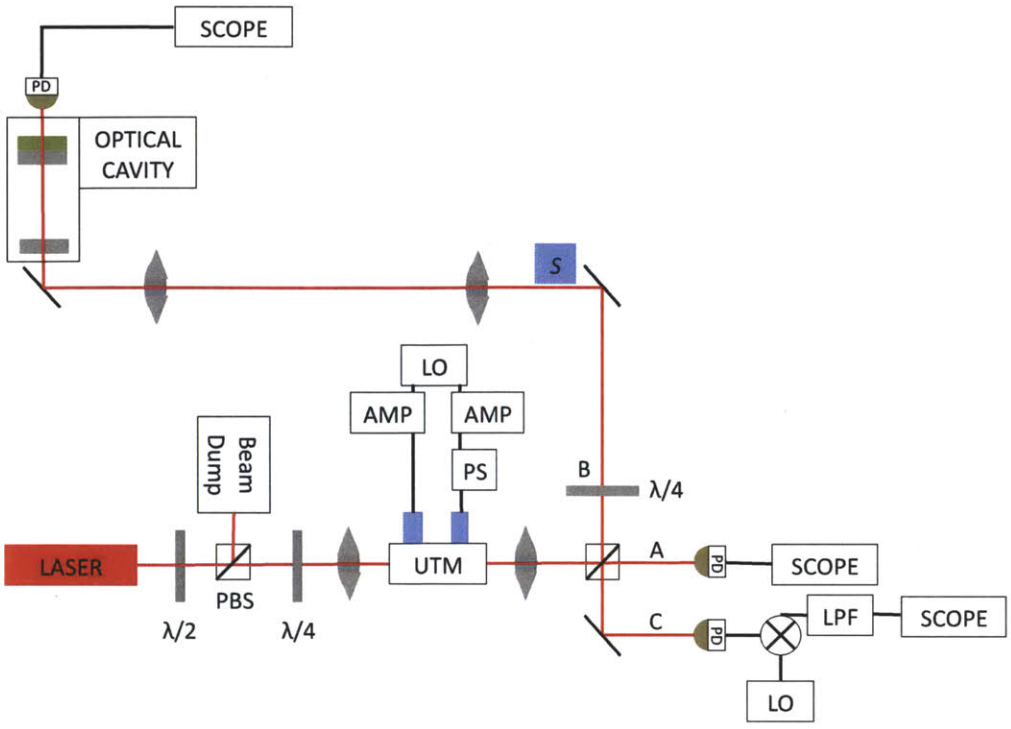

Figure 2-6: The experimental setup. The paths of the laser beam are indicated with the red lines. The UTM is shown with its attached electronics: The local oscillator (LO) at 25.23 MHz, the amplifiers (AMP), phase-shifting cable (PS), and the resonant tank circuits (blue rectangles). Components labeled PD are photodetectors, and LPF stands for lowpass filter. We differentiate between different paths: path A is used to measure the amplitude modulation strength, path B goes to the cavity, and path C measures the reflected signal from the cavity. We also note point S, which is roughly what was used as a "zero" point when doing the beam scan measurements for the mode matching.

modulation. Instead, we created two resonant circuits, which amplified the input voltages while keeping the power constant.

The overall circuit design, a standard tank circuit, is shown in Figure 2-7. It uses a transformer to boost up the input voltage by a factor of the turns ratio in L_1 to L_2. The toroids were bought from a selection of toroids of a variety of sizes and materials produced by Micrometals. The T68-17 toroids were eventually used because of their high Q at a frequency of 25 MHz (the frequency of the input signals), and because they were large enough to wind the necessary turns but small enough to fit in a small Pomona box.

The capacitance of the input ports (essentially the capacitance of the crystals) was measured to be 50 pF using an LCR meter. Because we wanted to create a resonant LC circuit, this input capacitance determined the value of L_2 in Figure 2-7, and thus the required number of windings. Micrometals gives a value of $2.1\,\mathrm{nH}/N^2$ for the T68-17 toroids. Therefore

$$N = \sqrt{\frac{1}{(2\pi \times 25\,\mathrm{MHz})^2(50\,\mathrm{pF})(2.1\,\mathrm{nH})}} \approx 20 \text{ turns} \tag{2.6}$$

An extra tunable capacitor C_{tune} was also soldered in parallel in order to adjust the circuit's resonant frequency more finely, since it was too difficult to get exactly the right inductance by winding.

The input signal passes through L_1. To get the highest voltage gain, we would like $\frac{N_2}{N_1}$ to be as high as possible, so the number of windings in L_1 should be as small as possible. However, we also want the circuit to be impedance matched as closely as possible to 50 Ω, which allows efficient power transfer with small reflections. The impedance seen by the input port is $Z' = \left(\frac{N_1}{N_2}\right)^2 Z$, which thus constrains N_1 since N_2 is already fixed.

The impedance of the circuit was measured using a 4195A HP Spectrum Analyzer. N_1 was carefully adjusted to get the impedance at 25 MHz equal to 50 Ω, and C_{tune} was adjusted to get the resonance frequency at 25 MHz.

The two crystal capacitances were slightly different, so two different resonant circuits were created in this manner. The resulting Q values were measured by looking at $f_{\mathrm{peak}}/2\Delta f$ as the spectrum analyzer swept through a range of frequencies around 25 MHz. The gain was measured by dividing the peak-to-peak output voltage by the peak-to-peak input voltage at 25 MHz. The final design resulted in Q values of 24 and 23 for the circuits.

2.3.2 The optical cavity

An over-coupled optical cavity was designed to test the reflected signal. This particular cavity was designed to have a flat input mirror of reflectivity $R_1 = 0.98$, and a

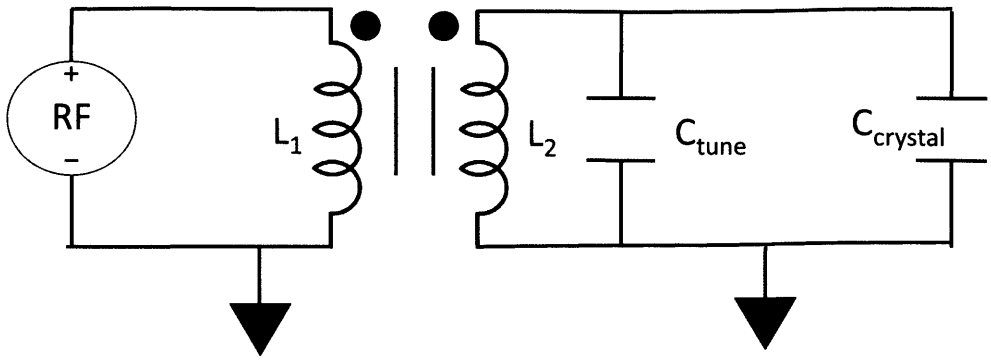

Figure 2-7: A circuit diagram for the resonant circuits.

second mirror with reflectivity $R_2 = 0.995$ and a radius of curvature $r = 20$ cm. With a cavity length of 10 cm, the cavity has a free spectral range (FSR) and finesse ($\mathcal{F}$) of

$$FSR = \frac{c}{2L} = 1.5\,\text{GHz} \tag{2.7}$$

$$\mathcal{F} = \frac{\pi\sqrt{R_1 R_2}}{1 - R_1 R_2} = 125 \tag{2.8}$$

The mount for the output mirror was constructed by epoxying three piezo-electric crystals to a two specially machined pieces, as shown in Figure 2-8. The piezos are elecrically connected to a voltage controller. The two mirrors were carefully placed at the correct position on the optics table and aligned to be parallel.

2.3.3 Mode Matching

Mode matching improves the coupling of light into a cavity by shaping the input beam such that it has a high (ideally, perfect) spatial overlap with one of the cavity's resonant transverse modes. The fundamental mode, which has a Gaussian intensity profile across its wavefront, is usually selected. The two parameters that can be adjusted at the input mirror are the radius of curvature of the wavefront and the size of the beam. Because of the shape of the cavity, as seen in Figure 2-10, we want the

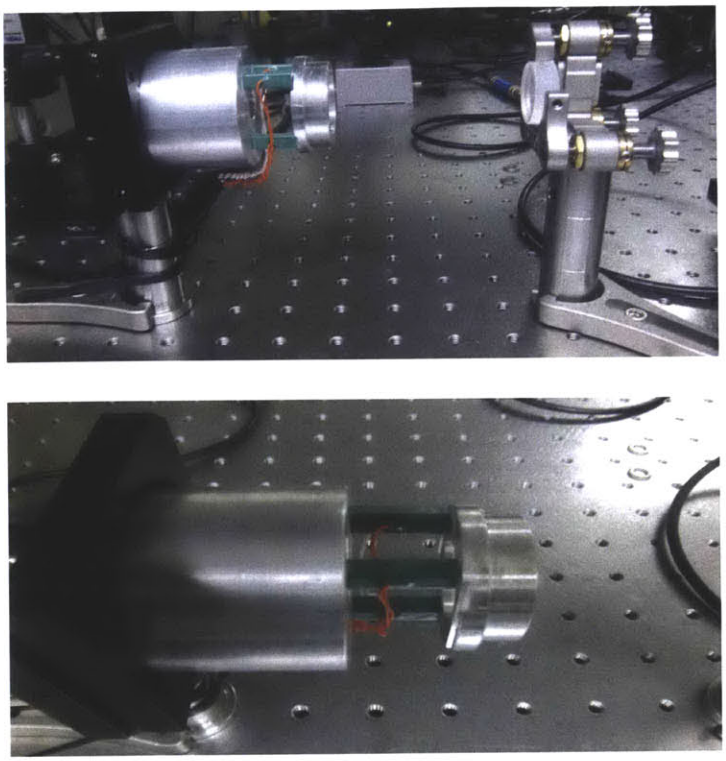

Figure 2-8: Top: The optical cavity is shown with the flat input mirror on the right and the output mirror on the left. Bottom: A closer look at the mount and its three piezos. They are placed in that pattern to allow the laser beam to pass through the center of the mirror.

input beam to be flat when it enters the cavity, with a size such that its radius of curvature matches that of the second mirror at $z = d$.

A beam propagating in the $\hat{z}$-direction can be nicely described in terms of its q-parameter, which encompasses both the radius of curvature $R_C(z)$ and the size of the beam, W(z) [9]:

$$\frac{1}{q(z)} = \frac{1}{R_C(z)} + i\frac{\lambda}{\pi W(z)^2} \tag{2.9}$$

where R_C and W are given by

$$R_C(z) = z\left(1 + \left(\frac{z_0}{z}\right)^2\right) \tag{2.10}$$

$$W(z) = w_0\sqrt{1 + \left(\frac{z}{z_0}\right)^2} \tag{2.11}$$

and z_0 is defined as

$$z_0 = \frac{\pi w_0^2}{\lambda} \tag{2.12}$$

w_0 is the smallest radius of the beam, as indicated in Figure 2-10. We choose a value of w_0 such that the equiphase surface of the beam coincides with the mirror surfaces of the cavity. Placing the input mirror at z = 0, we then require that the radius of curvature of the beam at the output mirror, at z = d, equal the radius of curvature of the mirror:

$$R_C(d) = 20\text{cm} = d\left(1 + \left(\frac{z_0}{d}\right)^2\right) \tag{2.13}$$

After solving for w_0, we can then easily calculate the waist of the input beam:

$$w_0 = \sqrt{\frac{\lambda}{\pi}\sqrt{dR_C(1 - \frac{d}{R_C})}} = \sqrt{\frac{1064\,\text{nm}}{\pi}\sqrt{10\,\text{cm} \times 20\,\text{cm}\left(1 - \frac{10\,\text{cm}}{20\,\text{cm}}\right)}} \approx 0.184\,\text{mm} \tag{2.14}$$

The input mirror is flat, so we want R(0) = ∞. The values for w_0 and R(0) enable us to calculate the q-parameter at the input mirror using Equation 2.9.

In order to create a mode-matched input beam, it was necessary to measure the beamwidth of the cavity input beam as a function of location on the optics table. Finding the waist of the beam would allow us to calculate the q-parameter of the input beam. However, the beam was well-collimated over the region where we were measuring, so we inserted a lens and then remeasured the beamwidth at 25.4 mm intervals beginning about 0.5 m before the input mirror at point S in Figure 2-6. A sample set of these measurements is shown in Figure 2-9. We then fit this data to the functional form for w(z) in Equation 2.11, obtaining the size of the waist, w_0, as well as its location z_w. The fit to W(z) of this data is also shown in Figure 2-9. We know the phase front of the beam is flat at the waist, so we can then use the fitted value w_0 to calculate the q-parameter at z_w.

We can then use the ABCD law for Gaussian beams [9] to back-propagate through free space and the lens to find the q-parameter of the input beam at point S. The ABCD law allows us to obtain the change in q as it propagates through an optical

system:

$$q_2 = \frac{Aq_1 + B}{Cq_1 + D} \tag{2.15}$$

where A, B, C, and D are the elements of the ray matrix for the optical system. The ray matrix describes the transition from an input vector (x_1, x_1') at a position z_1 along the optic axis to an output vector (x_2, x_2') at z_2 according to the equation

$$\begin{pmatrix} x_2 \\ x_2' \end{pmatrix} = \begin{pmatrix} A & B \\ C & D \end{pmatrix} \begin{pmatrix} x_1 \\ x_1' \end{pmatrix}$$

where x_i is the distance from the optic axis and $x_i' = dx_i/dz$. The properties of the optical system through which the beam propagates are encompassed by the parameters A, B, C, and D. For example, propagation through free space over a distance d is described by

$$\begin{pmatrix} 1 & d \\ 0 & 1 \end{pmatrix}$$

Propagation through a thin lens of focal length f is described by

$$\begin{pmatrix} 1 & 0 \\ -\frac{1}{f} & 1 \end{pmatrix}$$

Propagation through a thin lens and then free space is described by multiplying the two matrices in the order they were encountered. This allows us to obtain A, B, C, and D to use in Equation 2.15. This q-parameter at S and the desired q-paramater at the input were both entered into a mode-matching code along with a list of available lenses. The code uses the ABCD law as described above to simulate the propagation of the input q-parameter, and optimizes the placement of pairs of lenses such that the propagated input $q-$parameter matches the desired q-parameter at the input mirror. After we entered our parameters, the code returned a solution, specified by two lenses and their required placement on the optical table, with an expected overlap of one with the fundamental mode of the cavity. A convex lens of focal length 254 mm was placed 3.3 inches from point S, and a second convex lens of focal length 76 mm was

placed 15.4 inches after that. The beam shape as calculated by the code is depicted in Figure 2-11.

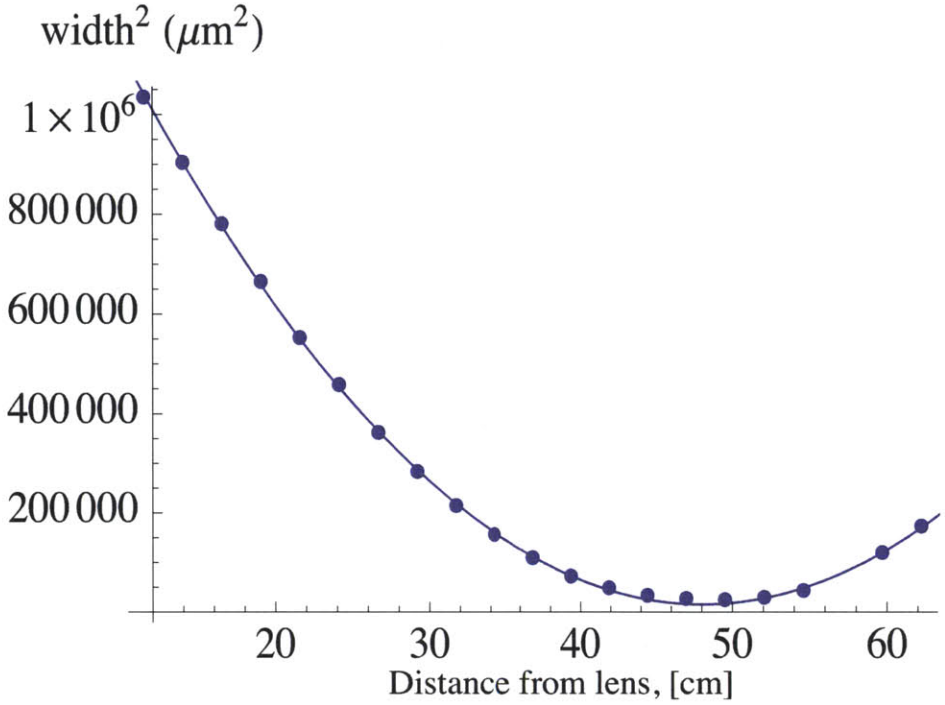

Figure 2-9: The measured beam widths and the corresponding fit of W(z).

2.3.4 The Error Signal

The reflected signal from the cavity can be calculated as follows. The laser beam acts as the carrier signal $c(t) = Ae^{i\omega_c t}$. The laser beam passes through the UTM, which modulates the amplitude with some modulation depth 2B/A, and the phase with some modulation depth y/A. Combining these two effects, we can write the incident field on the cavity as

$$E_{inc} = (A - 2B\sin(\omega_m t))e^{i(\omega_c t + y\sin(\omega_m t))} \tag{2.16}$$

We can then Taylor expand the phase modulation portion of the exponential, and

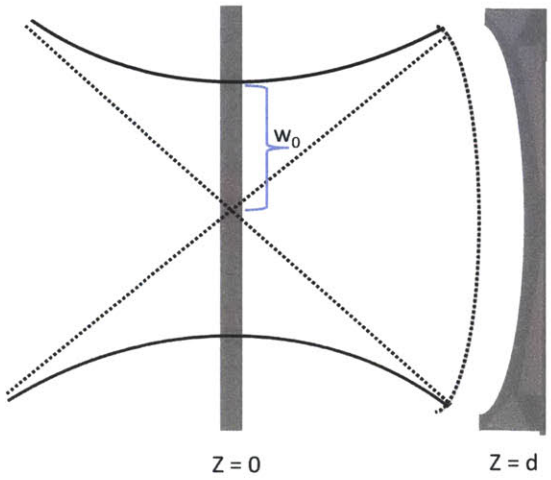

Figure 2-10: The cavity mirrors are shown along with the shape of the wavefronts for the fundamental mode to which we are trying to mode match. w_0 is indicated.

rewrite the sine functions in terms of exponentials:

$$(A + iB(e^{i\omega_m t} - e^{-i\omega_m t}))(1 + \frac{y}{2}(e^{i\omega_m t} - e^{-i\omega_m t}))e^{i\omega_c t} \tag{2.17}$$

We can expand this expression and separate it into terms with the same frequency. We can then compute the reflected field, E_{ref}, by multiplying each term by the corresponding reflection coefficient F(ω). In an critically coupled cavity F(ω) is given by

$$F'(\omega) = \frac{r(e^{\frac{2i\omega d}{c}} - 1)}{1 - r^2 e^{\frac{2i\omega d}{c}}} \tag{2.18}$$

However, it is important to note that in an over-coupled cavity, such as the one used in this experiment, F(ω) is instead given by

$$F(\omega) = \frac{-r_1 + r_2 e^{-i(\omega/c)2d}}{1 - r_1 r_2 e^{-i(\omega/c)2d}} \tag{2.19}$$

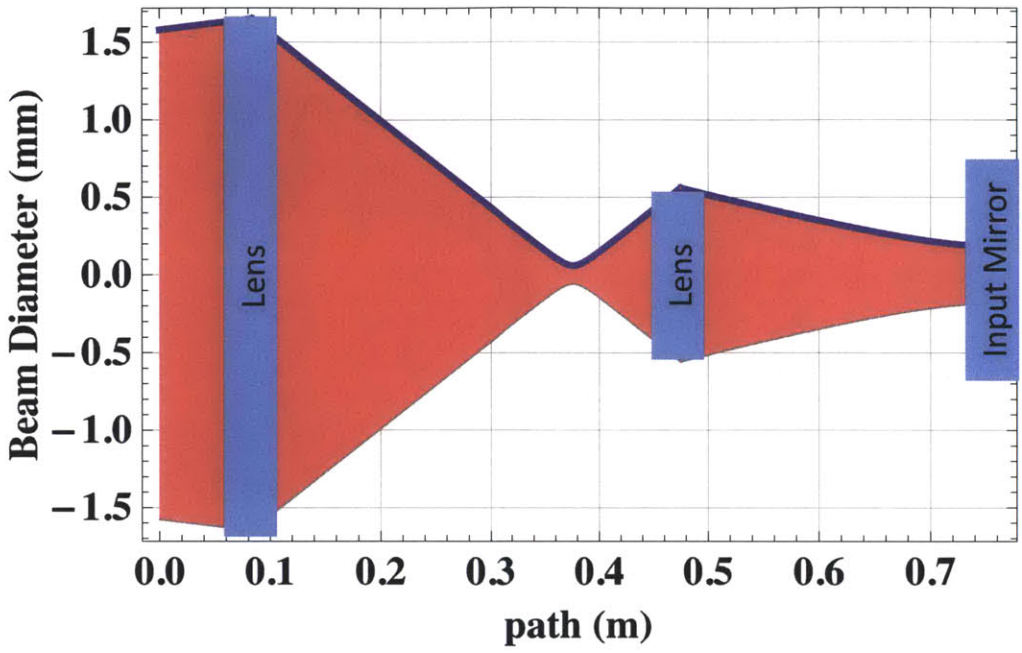

Figure 2-11: The shape of the solution calculated by the mode-matching code. The lenses and input mirror are indicated.

where $r_2 > r_1$. Using a different cavity will result in a different reflected field, and thus a different error signal. Note, for example, that $F(\omega) \rightarrow 1$ on resonance, but $F'(\omega) \rightarrow 0$. In any case, the reflected field E_{ref} is given by

$$\begin{aligned} E_{ref} = (A - iBy)F(\omega_c)e^{i\omega_c t} + (Ay/2 + iB)F(\omega_c + \omega_m)e^{i(\omega_c+\omega_m)t} \\ -(Ay/2 + iB)F(\omega_c - \omega_m)e^{i(\omega_c-\omega_m)t} + \frac{iBy}{2}F(\omega_c + 2\omega_m)e^{i(\omega_c+2\omega_m)t} \\ +\frac{iBy}{2}F(\omega_c - 2\omega_m)e^{i(\omega_c-2\omega_m)t} \end{aligned} \tag{2.20}$$

The reflected power is then given by $P_{ref} = E^*_{ref}E_{ref}$.

$$\begin{aligned} P = E^*_{ref}E_{ref} = [(A + iBy)F^*(\omega_c)e^{-i\omega_c t} + (\frac{Ay}{2} + iB)F(\omega_c + \omega_m)e^{-i(\omega_c+\omega_m)t} \\ -(\frac{Ay}{2} - iB)e^{-i(\omega_c-\omega_m)t}F^*(\omega_c - \omega_m) + 2\omega_m \text{ terms}] \times [c.c.] \end{aligned} \tag{2.21}$$

The reflected signal from the cavity is mixed with the local oscillator frequency ω_m and low-passed, so we can extract the terms in P that oscillate at ω_m.

$$P = 2\Re(x_1 - x_2)\cos(\phi) - 2\Im(x_1 + x_2)\sin(\phi) \tag{2.22}$$

where ϕ is the relative phase of the mixing signal, and where x_1 and x_2 are given by

$$\begin{aligned} x_1 &= (Ay - iB)(A - 2iBy)F(\omega_c)F^*(\omega_c + \omega_m) \\ x_2 &= (Ay - iB)(A - 2iBy)F(\omega_c)F^*(\omega_c - \omega_m) \end{aligned} \tag{2.23}$$

Using this calculated result, we can plot various signals based on the desired ratio of amplitude to phase modulation.

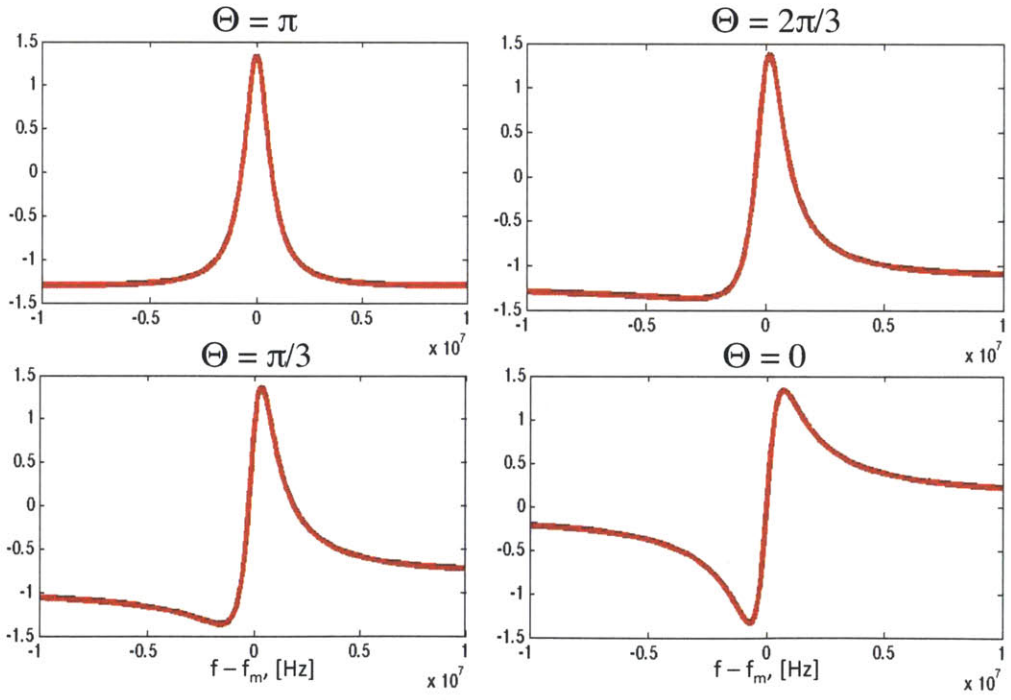

Figure 2-12: Reflected error signals are calculated using the reflection coefficient for overcoupled cavities for four different phase differences between the two input signals, shown here as $\theta = \pi, 2\pi/3, \pi/3$, and 0.

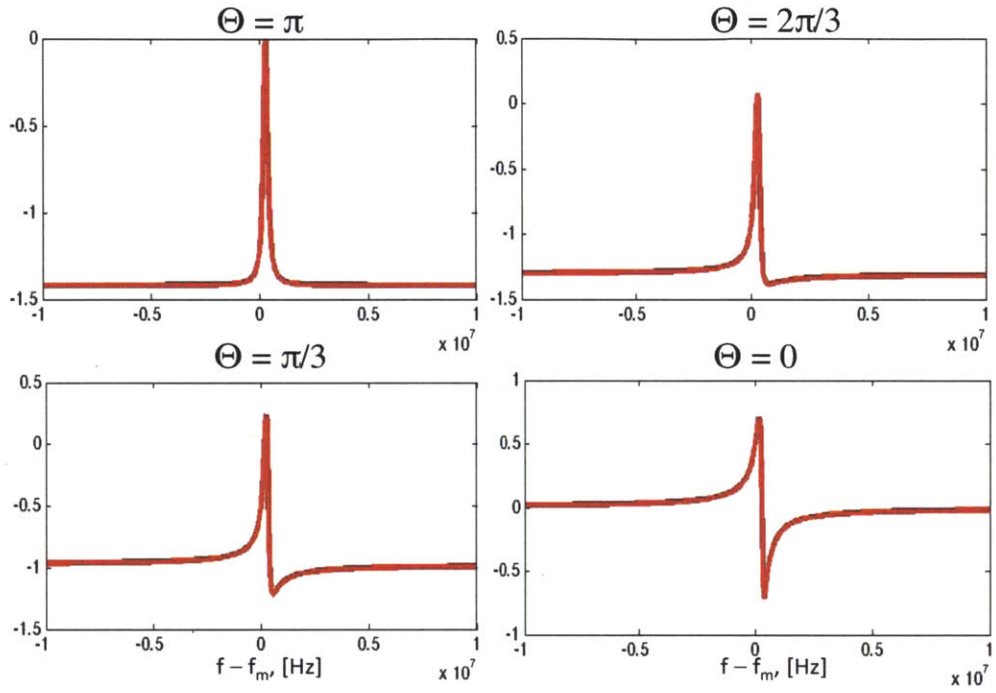

Figure 2-13: Reflected signals are calculated using the reflection coefficient for critically coupled cavities. The signals are quite different, most importantly in the change in offset of the amplitude modulated signal, which makes it much less useful in the locking method we would like to use since a DC offset would need to be added.

Chapter 3

Results and Conclusions

The shapes of the error signals measured from the cavity reflection matched the calculated signals. The cavity reflection was measured at several different relative phases between the input signals, corresponding to different ratios of AM to PM, as shown below. The measured reflected signals were fit to Equation 3.1 to determine the percentages of amplitude and phase modulation, as can be seen in Figure 3-1.

$$R(\omega) = 2A(-iM_{AM} + M_{PM})(F(\omega)F^*(\omega + \omega_m) + F(\omega)F^*(\omega - \omega_m)) \tag{3.1}$$

where, as explained previously, the reflection coefficient for the cavity is given by

$$F(\omega) = \frac{-r_1 + r_1(r_1^2 + t_1^2)e^{2i\omega d/c}}{1 - r_1 r_1 e^{2i\omega d/c}} \tag{3.2}$$

where r_i is the reflectivity of the input mirror, 0.98, and r_o is the reflectivity of the output mirror, 0.995. The measured data is taken with a cavity length changing at 20 Hz, and is in units of seconds, not frequency. We can do a simple change of variables:

$$\omega = \frac{s \times t}{2\pi} \tag{3.3}$$

where ω is frequency, s is the scanning rate of the cavity length, and t is time. We can then fit F(s$\times t/2\pi$) to obtain A, M_{AM}, and M_{PM}. The fractions of amplitude and

phase modulation are given by

$$\frac{M_{AM}}{M_{AM}+M_{PM}}, \qquad \frac{M_{PM}}{M_{AM}+M_{PM}} \tag{3.4}$$

respectively.

Using the full-width half-maximum of the transmission peak, the x-axis of these plots was converted from time to cavity linewidths from resonance. The measured signals do show some inconsistency with the calculations in that they change in amplitude and there is a slight offset (an offset parameter was added to the fits in order to obtain correct values for A, M_{AM}, and M_{PM}). The change in amplitude was improved by increasing the optical power by a factor of ten. The offset was most likely caused by RF AM, and was eliminated as described later in this section.

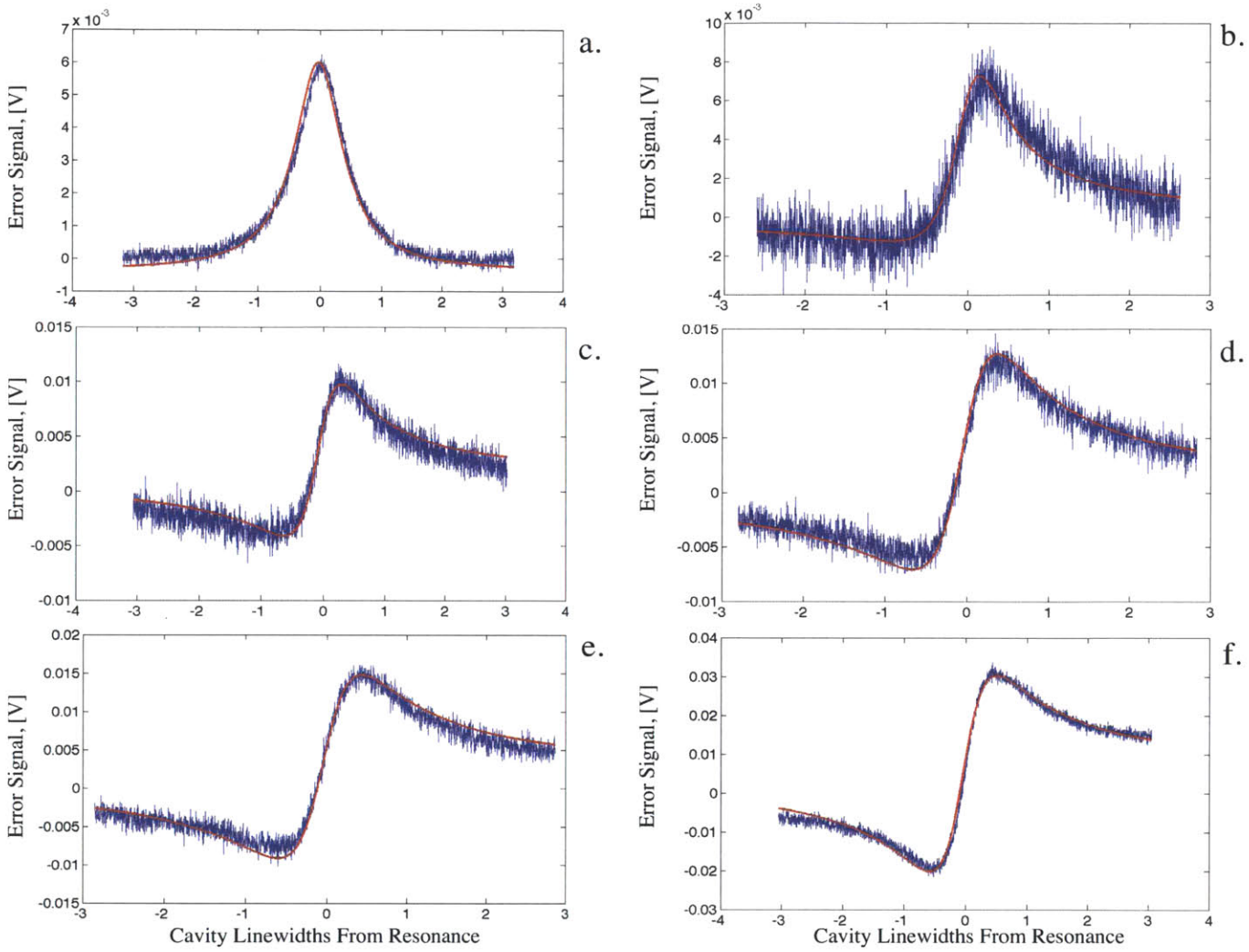

Figure 3-1: The error signals reflected from the cavity after being mixed with the local oscillator and sent through a low-pass filter. a. $P_{AM} = 100\%, P_{PM} = 0\%$ b. $P_{AM} = 50\%, P_{PM} = 50\%$ c. $P_{AM} = 20\%, P_{PM} = 80\%$ d. $P_{AM} = 15\%, P_{PM} = 85\%$ e. $P_{AM} = 10\%, P_{PM} = 90\%$ f. $P_{AM} = 0\%, P_{PM} = 100\%$

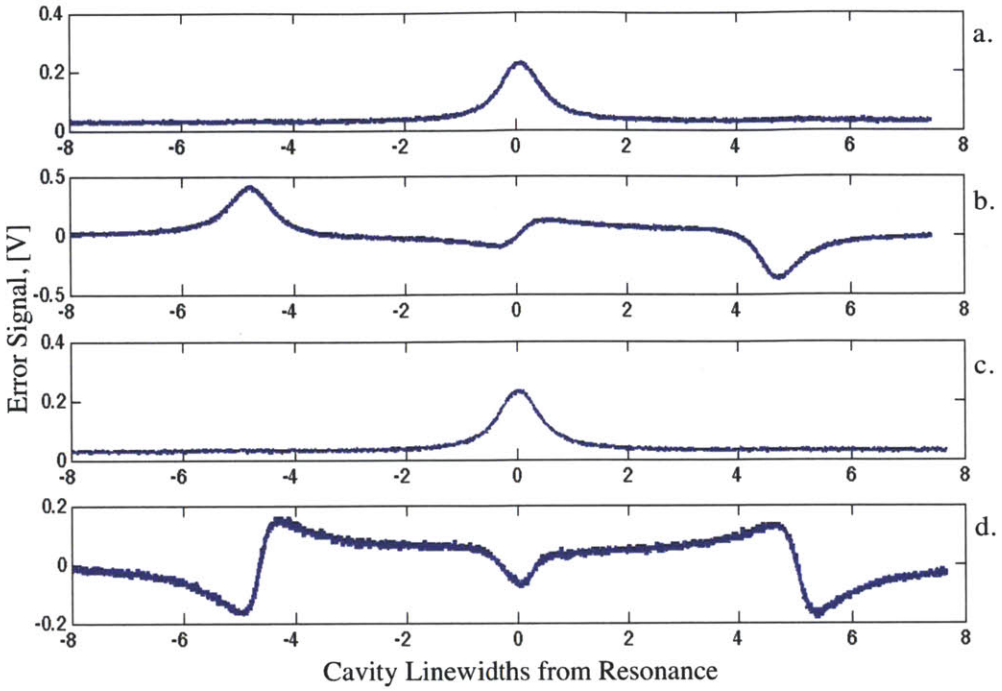

Figure 3-2: a. A nice example of the transmission for the reflected error signal in b. Pure amplitude modulation, zoomed out to include the sidebands (they are too small to see in the transmission spectrum but they create the two extra peaks in the reflected signal). c. A nice example of the transmission for the reflected error signal in d. Pure phase modulation, zoomed out to include the sidebands (they are too small to see in the transmission spectrum but they create the two extra peaks in the reflected signal). Additionally, the optical power has been increased by a factor of ten and the reflected signals for amplitude and phase modulation are now on the same order of magnitude in amplitude.

The zero-crossing of the error signal in each plot was extracted and plotted in cavity linewidths from resonance as a function of the percentage of phase modulation, as shown in Figure 3-3. Clearly, the zero-crossing moves from about half a linewidth off-resonance towards zero, indicating that the UTM will in fact be useful for locking cavities off-resonance and smoothly tuning the cavity length from its largest detuning at half a linewidth through all of the intermediate lengths until the resonant length is reached.

Another parameter of importance is the optical gain, which is essentially the slope of the reflected signal near the operating point (the zero-crossing). The slope

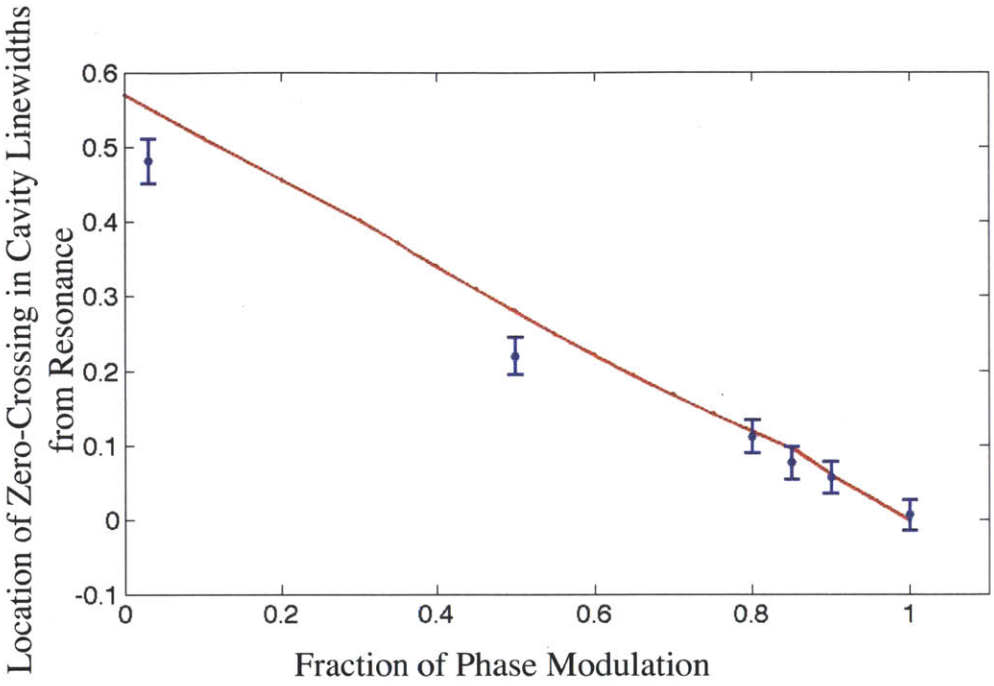

Figure 3-3: The zero crossing of the error signal as a function of the PM to AM ratio was extracted from the fitted plots and compared with calculated values, which match reasonably well.

corresponds to the voltage that the servo amplifier will apply to the piezo to adjust the cavity length by some Δd, and ideally it would be constant as the detuning is changed. Otherwise, the servo gain has to be adjusted to compensate, which is undesirable. We can calculate the optical gain we expect by taking the derivative of Equation 2.22 and evaluating it at the zero-crossing. As we can see in Figure 3-4, even the calculated optical gain is not constant, so the measurements for this curve need to be more closely spaced than the data points we currently have. Then the curve can be precisely mapped and the servo amplifier can be programmed accordingly. The phase-shifting circuits, as discussed below, will be immensely helpful in this case.

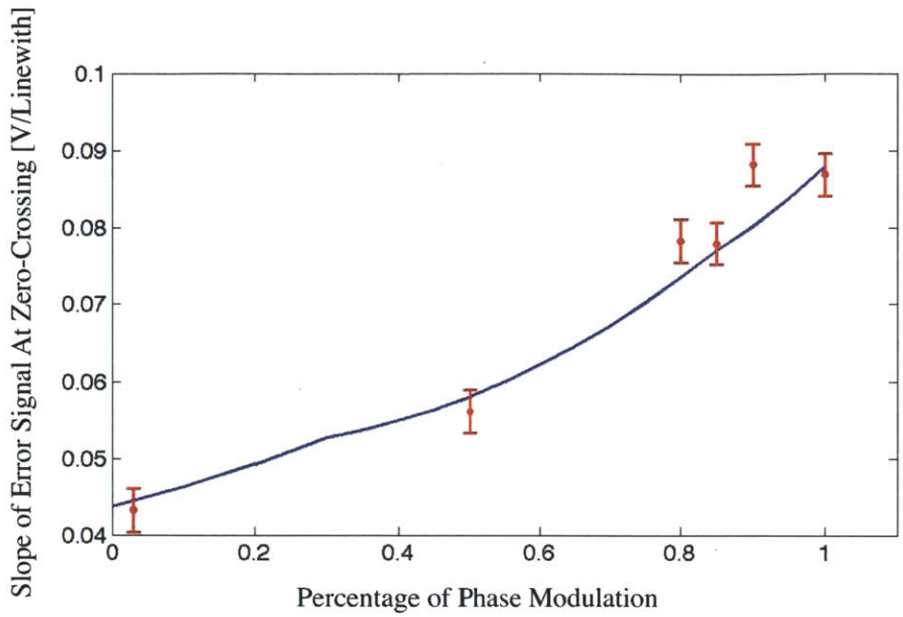

Figure 3-4: The optical gain as a function of the PM to AM ratio in a small region near the zero-crossing was extracted from the fits of Figure 3-1. The slopes were normalized by the fitted amplitudes, then compared to calculated values. They match reasonably well.

3.1 Future Work

3.1.1 Offsets

These measured error signals do have an offset, which was most likely due to RF AM, which can be eliminated through adjustment of the alignment through the UTM and of the input polarization of the light. By turning the quarter-wave plate before the UTM, the input polarization was adjusted and it was observed that the offset disappeared, as can be easily observed in Figure 3-5.

However, according to the transfer function of the UTM in Equation 2.2, adjusting the input polarization adjusts σ, so any input polarization that is not circular will favor either phase or amplitude modulation. After measuring the total amplitude modulation both before and after the quarter-wave plate was turned, it was clear

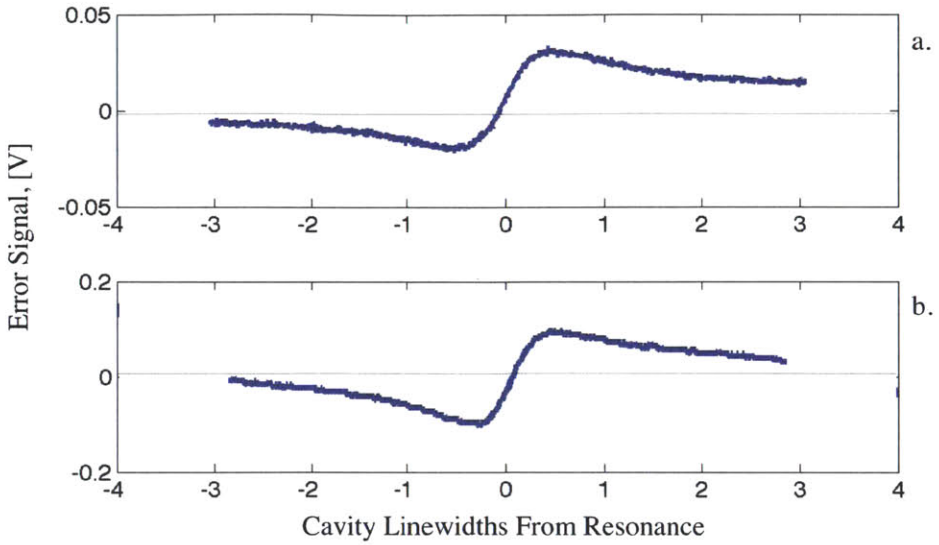

Figure 3-5: A phase modulated signal before and after the imput polarization was adjusted. The offset is visible when the input is circularly polarized, but disappears when the input polarization is adjusted.

that the amplitude modulation had been decreased, as can be observed in Figure 3-6.

It happens that the amplitude modulation lost through a change in the input polarization can be regained through a DC bias offset applied across the modulator's crystals. The current input polarization will be kept constant and we will explore the consequences of the DC bias, in particular trying to find the required voltage such that the original modulation depth can be regained. This will require the use of a bias T placed after the resonant tank circuits, as shown in Figure 3-7, because a DC voltage cannot be passed across a transformer. Additionally, because the tank circuits currently use the capacitance of the crystals to fulfill the resonance condition, new tank circuits will have to be built to account for the new input capacitance of the bias T.

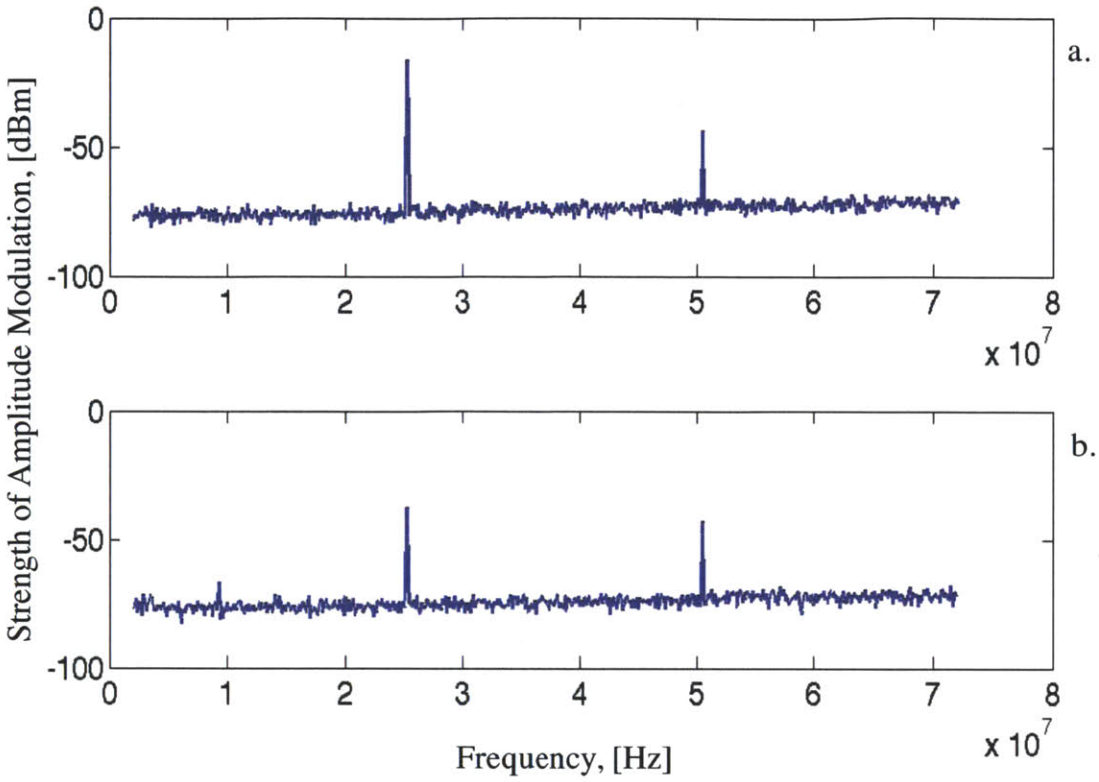

Figure 3-6: The amplitude modulation depth decreases when the input polarization is changed to eliminate the RF AM offset.

3.1.2 Phase Shifter

In addition to the bias T, there remains some further work to be done on this project before it can be used in the ponderomotive interferometer experiment. Phase-shifting with cable is tedious and makes it difficult to obtain a continuous shift of the zero-crossing. Certainly it would be impossible to switch between various cable lengths while trying to continuously detune a locked cavity. Phase-shifting circuit boards have been ordered for the purpose of replacing the cables. They consist of traces on a PCB that lengthen the path of the signal by multiples of 1/16 ns, which is .5625° at 25 MHz. The board contains multiples of 1/16 ns beween 1/16 ns and 16 ns, with a switch that allows the signal to take the longer or shorter path in each case, for a total

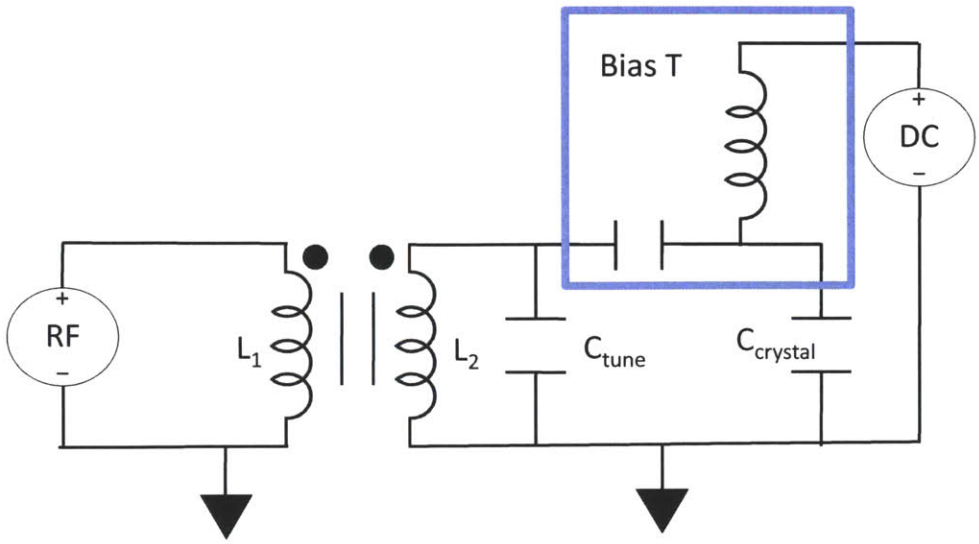

Figure 3-7: The resonant circuit, bias tee, and input crystal capacitance.

possible delay of 32 ns or 288°. The board will eventually be attached to a voltage controller that allows the phase shifting to occur in a consistent, pre-programmed manner. The small phase shift will allow for a more continuous measurement of the zero-crossing and optical gain as a function of detuning. When these steps are complete, the UTM can be optically integrated into the interferometer experiment and will hopefully be useful in some experimental measurements.

3.2 Closing Remarks

The data sets show that the UTM can modulate the laser light in such a way that purely amplitude modulated light, purely phase modulated light, and intermediate steps are easily produced by shifting the relative phase of the two voltage inputs. The zero-crossing moves smoothly from half a linewidth off-resonance to the resonance point of the cavity. While there are still steps to be taken before the UTM can be put

to use, it has already been shown to operate according to calculations because the shapes of the reflected error signals at different phase shifts match the corresponding calculated signals. The UTM provides an interesting and highly useful twist on the original Pound-Drever-Hall locking method, which will hopefully help to produce some new experimental results.

Appendix A

List of Electronic Components

1. Photodiodes
   (a) 1811 (3)
   (b) 1811 Power Supply and DC, AC cables (3)
2. Tank Circuits
   (a) T68-17 Micrometals toroids (2)
   (b) Pomona boxes (2)
   (c) Trim capacitors (2)
3. Cavity
   (a) PZT (3)
   (b) Thorlabs MDT693A 3-Axis Open Loop Controller
   (c) Function Generator
4. Various Electronics
   (a) Amplifiers ZFL-1000G (2)
   (b) Splitters (2)
   (c) Couplers (2)

(d) Mixers (1)

(e) Local oscillator (1)

(f) DC voltage source (3)

5. Misc Useful Tools

(a) Scope Probe (2)

(b) HP Spectrum Analyzer with Impedance measurement kit

(c) LCR meter

Bibliography

[1] Sarah Ackley. Construction and characterization of a universally tunable modulator. 2008.

[2] Eric D. Black. An introduction to pounddreverhall laser frequency stabilization. *Am. J. Phys.*, 69(79):79, January 2001.

[3] T. Corbitt, Y. Chen, E. Innerhofer, H. Mller-Ebhardt, D. Ottaway, H. Rehbein, D. Sigg, S. Whitcomb, C. Wipf, and N. Mavalvala. An all-optical trap for a gram-scale mirror. *Phys. Rev. Lett.*, 98(15):150802, April 2007.

[4] T. Corbitt, Y. Chen, F. Khalili, D. Ottaway, S. Vyatchanin, S. Whitcomb, and N. Mavalvala. Mathematical framework for simulation of quantum fields in complex interferometers using the two-photon formalism. *Phys. Rev. A*, 73(2):023801, February 2006.

[5] T. Corbitt, Y. Chen, and N. Mavalvala. Mathematical framework for simulation of quantum fields in complex interferometers using the two-photon formalism. *Phys. Rev. A*, 72(1):183818, July 2005.

[6] T. Corbitt, C. Wipf, T. Bodiya, D. Ottaway, D. Sigg, N. Smith, S. Whitcomb, , and N. Mavalvala. Optical dilution and feedback cooling of a gram-scale oscillator to 6.9 mk. *Phys. Rev. Lett.*, 99(16):160801, October 2007. This is a full ARTICLE entry.

[7] B. Cusack, B. Sheard, D. Shaddock, M. Gray, P. Lam, and S. Whitcomb. Electro-optic modulator capable of generating simultaneous amplitude and phase modulations. *Applied Optics*, 43(26):5079–5091, September 2004.

[8] R. W. P. Drever, J. L. Hall, F. V. Kowalski, J. Hough, G. M. Ford, A. J. Munley, and H. Ward. Laser phase and frequency stabilization using an optical resonator. *Appl. Phys. B*, 31(2):97–105, February 1983.

[9] Joseph T. Verdeyen. *Laser Electronics.* Prentice-Hall, 1981.

[10] Amnon Yariv. *Quantum Electronics.* John Wiley and Sons, Inc., 1967.